Hindawi
Geofluids
Volume 2021, Article ID 5574713, 12 pages
https://doi.org/10.1155/2021/5574713

Research Article

Physical Simulation Test on Temperature Field Distribution of Artificial Vertical Straight Multirow Freezing Inclined Shaft

Jielong Sun[1] **and Jianxi Ren**[2]

[1]*School of Architecture and Civil Engineering, Yan'an University, Yan'an Shaanxi 716000, China*
[2]*School of Architecture and Civil Engineering, Xi'an University of Science and Technology, Xi'an 710054, China*

Correspondence should be addressed to Jielong Sun; sunjielong@yau.edu.cn

Received 29 January 2021; Accepted 4 June 2021; Published 21 June 2021

Academic Editor: Jinze Xu

This study investigated the temperature field distribution of a freezing inclined shaft. Thus, a three-dimensional physical simulation test system was developed, and the system consists of six parts, which are simulation box and shaft model, loading system, freezing system, external environment simulation system, and data acquisition system. From the results of physical and mechanical property test of artificially frozen sand, in the range of 25°C to -20°C, the heat capacity of sand decreases first, then increases, decreases, and finally tends to be stable; the thermal conductivity of sand gradually increases and finally becomes stable; and the cohesion, internal friction angle, uniaxial compressive strength, and elastic modulus of artificially frozen sand all increase as the freezing temperature decreases. The three-dimensional physical simulation test and field measurement showed that the distance from the freezing pipe is the main factor affecting freezing wall temperature, and the closer to the freezing pipe, the faster the cooling rates. Comparison of theoretical calculation results and field measurement results shows that the calculation formula of freezing wall temperature with time of the inclined shaft can reflect the general law of freezing wall temperature cooling. Therefore, the 3D physical simulation test system is reliable and the test method is feasible.

1. Introduction

Vertical straight-line artificial freezing is often used to excavate a shaft in areas with large water content, shallow coal seam, and soft soil [1]. However, if the strength of the frozen wall is not enough in the process of sinking, the accidents of water gushing and sand flooding are likely to occur, which will pose a threat to the safety of human life and bring substantial economic losses at the same time [2–13]. To ensure that the inclined shaft can safely cross the water-rich soft soil stratum, the formation speed and thickness of the frozen wall must be studied in depth, and the temperature of the freezing wall can directly reflect the formation speed and thickness of the frozen wall.

At present, some researches have been carried out on the temperature field of the frozen wall, among which Cao et al. [14] studied the adaptability of the freezing method under the condition of water-rich sandy pebble stratum and the rationality of the freezing design scheme. Yang et al. [15] studied the characteristics of the artificial freezing tunnel model test and prediction of the surrounding rock temperature field. Li [16] studied the freezing temperature field and the thermal conductivity of two representative soils and analyzed the numerical simulation of freezing temperature with the equivalent thermal conductivity tested using the ANSYS software. Liu et al. [17] used scale model tests and numerical simulation and analyzed the artificial freezing at different temperatures in complicated strata. Hu and Zhao [18] studied the precision of the Bakholdin model for the temperature field of artificial ground freezing. Lü [19] analyzed the temperature variation law based on the thermodynamics theory and the phase change law of frozen soil. Hu et al. [20] established artificial ground freezing temperature field models to study the effect of the soil freezing point on the calculation of frozen wall thickness. Wang et al. [21] used a self-made test device to study the laws of the temperature field and obtain the information for predicting the frost heave and numerical simulation of the artificially frozen soil. Zhang

and Yu [22] used the finite element method to analyze the formation and temperature distribution of the freezing wall in the artificial freezing method. Fan and Yang [23] present a detailed case study of a cross passage, including the temperature variations in brine and selected monitoring points around the passage based on the field testing results during freezing and frozen wall maintenance. Shen et al. [24] studied the influence of temperature and moisture content on sandstone thermal conductivity from a case using the artificial ground freezing (AGF) method. Gianpiero et al. [25] studied the artificial ground freezing technique to excavate a tunnel below the ground water table. Feng et al. [26] simulated the freezing process of artificially frozen soils of the Dalian Road tunnel connecting the passage with the finite element analysis method and worked out the varying laws of temperature fields, displacement fields, and stress fields. Vitel et al. [27] studied the modeling heat transfer between a freeze pipe and the surrounding ground during artificial ground freezing activities. Young et al. [28] studied the finite element modeling and analysis for artificial ground freezing in egress shafts. Ji et al. [29] present a model based on 2D heat conduction and calculate the temperature distribution in the frozen wall. Lackner et al. [30] studied the artificial ground freezing of fully saturated soil: thermal problem. Wang et al. [31] studied the influence of the temperature field of the frozen wall on the temperature field of hydration heat of the outer wall and obtained the basic law of temperature change of the outer wall and freezing wall during sinking in extrathick alluvium. Hou et al. [32] studied the frozen temperature field distribution law of multirow pipes in large cross-sectional inclined shaft construction. Wang and Yang [33] established a plane finite element model to simulate the whole process of ground frozen-shaft excavation-thawing. Through the sequential coupling of the temperature field and stress field, the stress law of the frozen wall during thawing in the surface soil section was obtained. Liu et al. [34] studied the formation and development of the frozen wall under the vertical straight-line frozen condition of water-bearing sand stratum and studied the distribution law of the frozen wall temperature field in the inclined shaft. Yao et al. [35] established a calculation model of the artificially frozen soil temperature field, which is based on the support vector machine algorithm, and gave a kernel function suitable for the temperature field. Zhang et al. [36] studied the transient temperature field of frozen soil with distributed optical fiber. The results showed inverse correlation and the nonmonotonic correlation between the temperature change rate of normal frozen soil and its initial water content. Li and Xia [37] based on the exponential integral function studied the temperature field of artificially frozen soil and obtained the theoretical expression of the thickness, velocity, and freezing time of the frozen soil curtain. Ren et al. [38] studied the mechanical properties and temperature field of the frozen wall in the water-rich sand layer by the combination of indoor physical mechanics test, field measurement, and finite element numerical simulation. He et al. [39] through numerical simulation analysis and field monitoring data studied the development law of the temperature field and frozen wall during the freezing process. Sheng and Wei [40] measured the multicircle temperature field of the frozen wall and analyzed the problems of the shallow section, deep freezing, and waste of cold energy and slow excavation speed of the frozen shaft in the early stage. Based on the actual parameters of the project, R. Wang and W. Wang [41] considered the phase change of water in the soil layer and the variation of frozen temperature with freezing time. The formation of the frozen wall and its temperature field characteristics under oblique conditions were analyzed in detail by using large-scale finite element software.

Table 1: The stratum of the freezing cross.

Stratum	Cumulative depth (m)	Layer thickness (m)	Name
Q_4^{eol}	7.60	7.60	Silt
Q_3s	16.83	9.23	Fine sand
Q_3s	25.30	8.47	Medium sand
Q_3s	33.60	8.30	Silt
Q_3s	72.20	38.60	Fine sand
Q_3s	79.10	6.90	Silt
Q_3s	97.60	18.50	Fine sand
Q_2l	98.90	1.30	Loess
J_2a	110.33	11.43	Sandy mudstone
J_2a	112.30	1.97	Medium-grained sandstone

However, the research on the temperature field of the frozen wall has achieved certain results, but the research on the distribution law of the temperature field in the vertical straight-line artificially frozen inclined shaft is still rare. In order to study the temperature field distribution of the freezing inclined shaft, this paper based on the freezing engineering of a main inclined shaft in northern Shaanxi completed an experimental study on the physical and mechanical properties of artificially frozen sand and three-dimensional physical simulation test of temperature field distribution law of artificially frozen inclined shaft, and according to the characteristics of freezing inclined shaft sinking, a set of three-dimensional physical simulation test system was developed. The results can provide some references for similar projects.

2. Engineering Background

The research is based on the artificially frozen method of the main inclined shaft in the Yuan Datan coal mine of northern Shaanxi. The length of the main inclined shaft is 1303.3 m, the inclination angle is 14°, the net section is 16.3m^2, the net width is 5.0 m, the wall height is 1.25 m, and the arch height is 2.5 m. In the upper section, the frozen method is used to sink the shaft. The frozen starting position is 80.215 m apart from the wellhead, the total inclination length of the frozen section is 377 m, the horizontal length is 365.8 m, and the vertical depth of the frozen shaft is 20 m to 111.3 m. Table 1 indicates the stratum of the freezing cross.

The pumping test estimated that water inflow from the main inclined shaft was 1250 m^3/h. Vertical straight-line artificial freezing is used for sinking an inclined shaft. There are 5 frozen holes in each row, and the spacing is 2.35 m. The

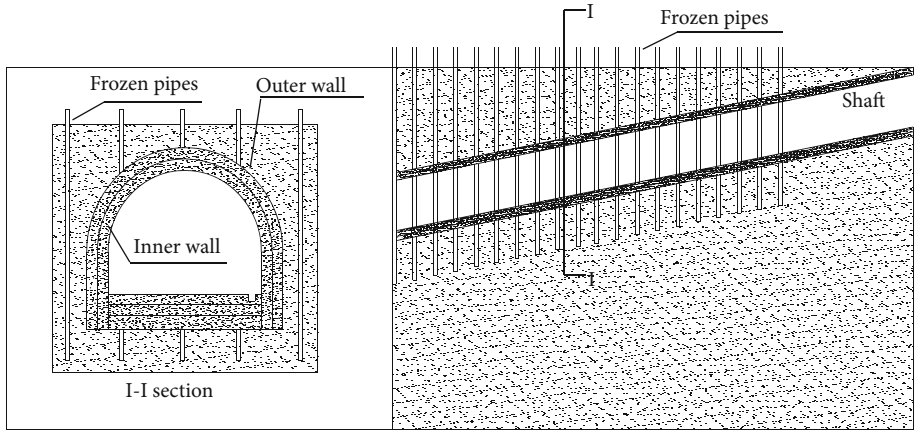

Figure 1: Inclined shaft cross section with frozen pipes.

designed thickness of the frozen wall is 6.0 m on the roof, 3.0 m on both sides, and 5.0 m on the bottom plate. Figure 1 indicates the layout of frozen holes.

3. Experimental Studies on Physical and Mechanical Properties of Artificially Frozen Sand

3.1. Thermal Physical Properties of Artificially Frozen Sand. The Test Protocol Hot Disk TPS 2500S thermal constant analyzer is the equipment used in the test, shown in Figure 2.

After sampling on site (buried depth is 60 m), it shall be prepared according to *Test Methods for Geotechnical Test Methods*. The prepared samples were grouped and put into the refrigeration box. The tests of specific heat capacity and thermal conductivity of sand at different low temperatures (25°C, -5°C, -10°C, -15°C, and -20°C) were completed successively. Figure 3 shows the results.

Figure 3(a) gives the specific heat capacity of sand at different low temperatures. It shows that the specific heat capacity decreases first, then increases, decreases, and finally tends to be stable with the decrease in temperature. When temperature cools from 25°C to -5°C, the free water in sand changes into ice and the specific heat capacity of ice is only about half of the water, so the specific heat capacity of sand is reduced. When temperature cools from -5°C to -10°C, the specific heat capacity of sand increases, because the free water velocity in the sand is condensed into the ice with temperature decreasing, and the internal energy required to be released in this process is larger. The specific heat capacity is reduced as internal energy is released by the free water condensed into ice when temperature cools from -10°C to -15°C. Since the internal energy released by the free water condensed into ice at unit temperature is unchanged, the specific heat capacity of sand is stable when temperature cools from -15°C to -20°C.

Figure 3(b) shows that the thermal conductivity of sand changes with temperature mainly in three stages: slow increase stage, rapid increase stage, and basic stability stage. As the temperature decreases, the contact between particles becomes closer and the heat conduction resistance, leading to the thermal conductivity, increases slowly when temperature cools from 25°C to -5°C. As the shrinkage intensified, the heat conduction resistance rapidly reduced and the thermal conductivity of sand increases rapidly when temperature cools from -5°C to -10°C. The temperature cools from -10°C to -20°C. The shrinkage of mineral particles reaches the extreme value; the heat conduction resistance and the thermal conductivity are unchanged.

Figure 2: Test Protocol Hot Disk TPS 2500S.

3.2. Mechanical Property Test of Artificially Frozen Sand

3.2.1. The Variation of Friction Angle and Cohesion of Sand under Different Frozen Temperatures. The samples were prepared according to *Test Methods for Geotechnical Test Methods*, and then, group samples before putting them into the refrigeration box. The direct shear test of sand under different low temperatures (-5°C, -10°C, -15°C, and -20°C) was carried out in sequence, and the test results are shown in Figure 4.

Figure 4 shows that as the frozen temperature is continuously decreased, the cohesion and internal friction angle of artificially frozen sand gradually increase. The cohesion and internal friction angle of artificially frozen sand increased about 0.98 times and 0.12 times when temperature cools from -5°C to -10°C. Figure 4(a) shows that the cohesion of artificially frozen sand increased about 0.26 times as temperature cools from -10°C to -15°C, and it can be seen that the cohesion of artificially frozen sand will increase with the

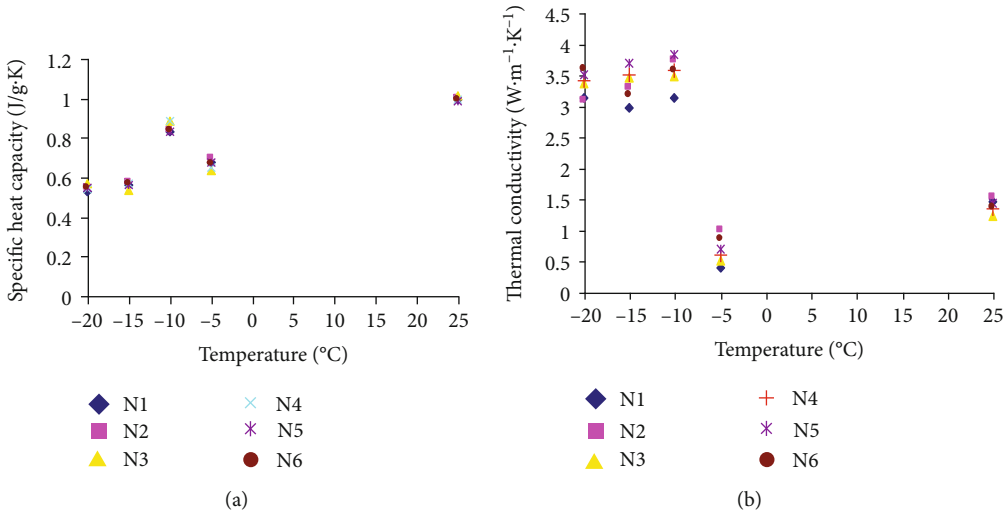

Figure 3: The specific heat capacity (a) and thermal conductivity (b) of sand at different temperatures.

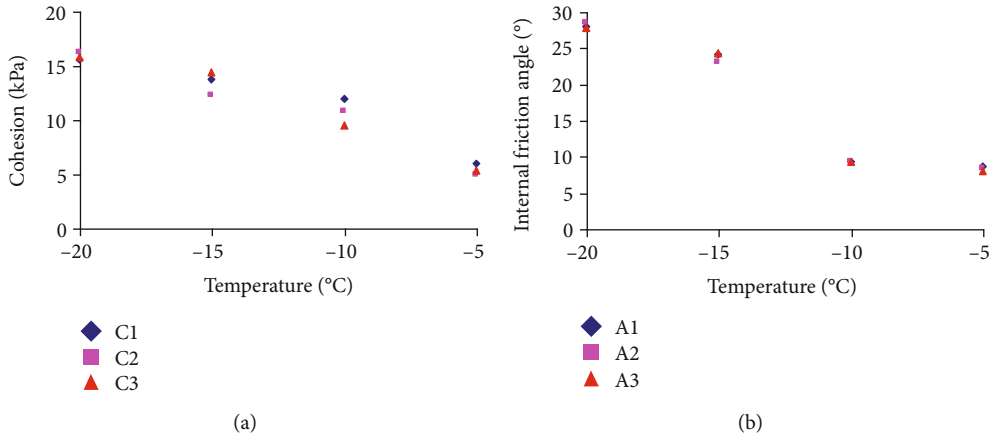

Figure 4: The cohesion (a) and internal friction angle (b) of sand at different temperatures.

decrease in frozen temperature. However, due to free water in sand condensed into ice, the increase range will gradually decrease. According to Figure 4(b), the internal friction angle of artificially frozen sand increases with the decrease in frozen temperature, and its increase amplitude becomes larger, since the cementing force is between the particles of the artificially frozen sand.

3.2.2. Uniaxial Compressive Strength Variation of Sand at Different Frozen Temperatures. The uniaxial compression test results of sand at different frozen temperatures (-5°C, -10°C, -15°C, and -20°C) are shown in Figure 5. According to Figure 5, the uniaxial compressive strength of artificially frozen sand increased from 3.83 MPa to 7.05 MPa, increasing by 0.84 time, when the frozen temperature is cooling from -5°C to -10°C (s). The uniaxial compressive strength of artificially frozen sand increases from 7.05 MPa to 14.18 MPa, when the frozen temperature cools from -10°C to -15°C, which was doubled. The uniaxial compressive strength of artificially frozen sand increases from 14.18 MPa to 15.64 MPa, increased by 0.1 times, when the frozen temperature cools from -15°C to -20°C. In summary, the uniaxial compressive strength of artificially frozen sand will gradually increase with the decrease in frozen temperature within -5°C to -20°C, and the growth rate is about 0.29~1.43 MPa/°C. The increased amplitude of the uniaxial

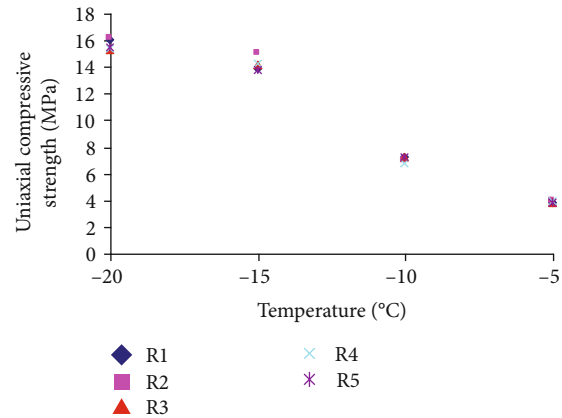

Figure 5: The uniaxial compressive strength of sand at different temperatures.

1 is temperature control system, 2 is appearance of incubator, 3 is refrigerator, 4 is interior of incubator.

(a) External environment simulation system

1 is cold-liquid inlet, 2 is cold-liquid outlet, 3 is frozen pipes.

(b) Frozen system

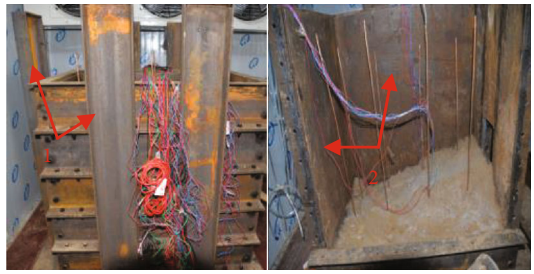

1 is reaction device, 2 is loading plate.

(c) Simulation box and loading system

1 is static strain gauge, 2 is optical sensing interrogator, 3 is vibrating string reader.

(d) Data acquisition system

Figure 6: Three-dimensional physical simulation system of the frozen inclined shaft.

compressive strength is most remarkable when the frozen temperature cools from -10°C to -15°C. However, the increased amplitude of uniaxial compressive strength is smallest when frozen temperature cools from -15°C to -20°C.

4. Three-Dimensional Physical Simulation Test of Vertical Straight-Line Artificially Frozen Inclined Shaft

According to the characteristics of the inclined frozen method, a three-dimensional physical simulation system for a frozen inclined shaft was developed. The system includes the external environment simulation system, frozen system, simulation box and loading system, and data acquisition system (Figure 6).

4.1. Physical Simulation Test Design

4.1.1. Similar Material Selection. The physical simulation test is an effective method to solve complex problems, and similar materials are the key to the simulation test. The similar material used in this simulation is typical sand in the frozen section of the inclined shaft, and its thermal physical parameters at different temperatures are shown in Table 2.

The similar material used in this study is typical sand of the inclined shaft. The density reduction ratio, specific heat capacity reduction ratio, thermal conductivity reduction ratio, and freezing latent heat ratio of water are shown in

Table 2: Thermophysical parameters of sand at different temperatures.

Density (kg/m^3)	Temperature (°C)	Heat capacity (kJ/(kg·°C))	Thermal conductivity (W/(m·°C))
2190	25	0.998	1.41
	-5	0.667	1.71
	-10	0.849	3.58
	-15	0.553	3.65
	-20	0.546	3.67

$$\begin{cases} C_\rho = \dfrac{\rho}{\rho'} = 1, \\ C_C = \dfrac{C}{C'} = 1, \\ C_\lambda = \dfrac{\lambda}{\lambda'} = 1, \\ C_Q = \dfrac{Q}{Q'} = 1. \end{cases} \quad (1)$$

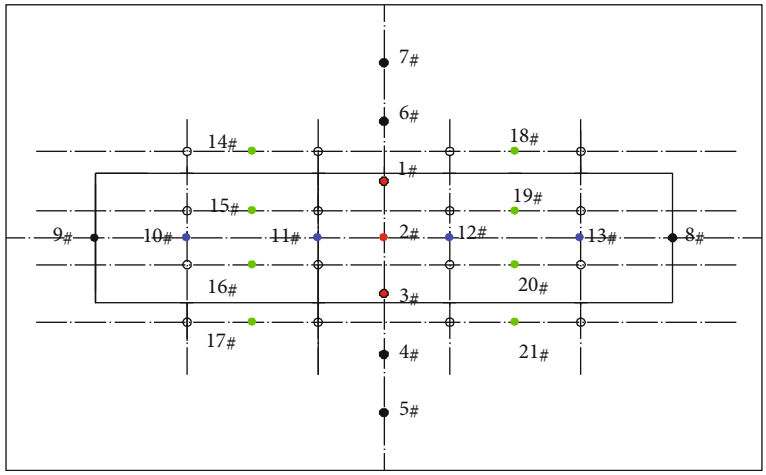

Figure 7: Schematic diagram of temperature measurement point layout.

In Formula (1), ρ and ρ' are the density of the prototype material and physical model material (kg/m^3), respectively; C and C' are the heat capacity of the prototype material and physical model (J/(kg·°C)), respectively; λ and λ' are the thermal conductivity of the prototype material and physical model (W/(m·°C)), respectively; and Q and Q' are the latent heat of freezing water of the prototype material and physical model (kJ/m^3), respectively.

4.1.2. Geometric Scaling. The model length, width, and height are 1 m, 0.6 m, and 1 m, respectively. According to Saint-Venant's principle, the soil within 3~5 times of tunnel diameter should be selected as the research object. According to the size of the 3D physical model table, the shaft wall is reversely pushed out and scaled according to a geometric ratio of 1 : 50. Thus, the clear width of the shaft wall model is 100 mm, the wall height is 25 mm, and the arch height is 50 mm. In the physical simulation test, the seamless copper pipe with a diameter of $\Phi 6.35 \times 0.7$ mm is used for the freezing pipe, and the row spacing is 42×200 mm.

4.1.3. Temperature Scaling. According to the Kosovitch criterion, temperature scaling can be expressed as

$$\begin{cases} \dfrac{Q}{C\rho T} = \dfrac{Q'}{C'\rho' T'}, \\ C_T = \dfrac{T}{T'}. \end{cases} \tag{2}$$

In Formula (2), T and T' are the temperature of the prototype material and physical model (°C), respectively, and C_T is the temperature scaling.

Substituting Equation (1) into Equation (2), one can obtain $C_T = T/T' = 1$, which means that the temperature of the prototype is consistent with that of the physical simulation test.

4.1.4. Time Scaling. According to the Fourier criterion, time scaling can be expressed as

$$\begin{cases} \dfrac{\lambda t}{C\rho R^2} = \dfrac{\lambda' t'}{C'\rho' R'}, \\ C_t = \dfrac{t}{t'}. \end{cases} \tag{3}$$

In Formula (3), t and t' are the time of the prototype material and physical model (s), respectively, and C_t is the time scaling.

Substituting Equations (1) and (2) into Equation (3), one can obtain $C_t = 2500$.

4.2. Layout of Measuring Points. The test data acquisition system adopts automatic monitoring, which consists of a fiber optic temperature sensor, data collector, and computer. The measuring point arrangement is shown in Figure 7. A total of 21 temperature monitoring points were arranged in the test. The red measuring points ($1_\#$ to $3_\#$) are affected by tangential and axially adjacent four frozen pipes, which were recorded as monitoring section I. The six black points ($4_\#$ to $9_\#$) were used to monitor the change of temperature in the edge zone, which were recorded as monitoring section II. The four blue measuring points ($10_\#$ to $13_\#$) are affected by two adjacent frozen tubes, which are recorded as monitoring section III. The eight green points ($14_\#$ to $21_\#$) under the influence of two axial adjacent frozen pipes are recorded as monitoring section IV.

The frozen system will be started after the data of each measuring points are stabilized, and then, record the data of each sensor. The intersection of the frozen wall surface with different running times during the frozen process is shown in Figure 8.

4.3. Analysis of Test Results

4.3.1. Variation Law of Cold Source Temperature. The stability of the cold source is one of the important factors to ensure

(a) Boot 2 h (b) Boot 4 h (c) Boot 8 h

(d) Boot 10 h (e) Boot 24 h (f) Boot 48 h

(g) Boot 72 h (h) Boot 96 h (i) Boot 120 h (stop frozen)

(j) Shutdown 24 h (k) Shutdown 48 h (l) Shutdown 72 h

Figure 8: Surface intersection of the frozen wall.

the stable development of the frozen wall. Therefore, before analyzing the temperature distribution law of the inclined shaft frozen wall, the variation law of the cold source in the freezing process should be firstly analyzed. Figure 9 shows the results.

According to Figure 9, the temperature of the cold source decreases rapidly from 0 to 6 hours after the test starts, and the temperature cools from 0°C to 27°C at 4.5°C/h. At 26h, the temperature of the cold source dropped from 27°C to a set temperature of -30°C and was maintained for 10 h. Now, the temperature of each monitoring section reaches -10°C, and the test changes from the active freezing period to the maintenance freezing period. The maintenance freezing temperature is set to -20°C. The cold source temperature began to rise within 36~42 h due to the change of the temperature setting value and stabilized at 56 h. The test entered the maintenance freezing period. The freezing is stopped at 120 h, and the temperature difference of desalinated brine during

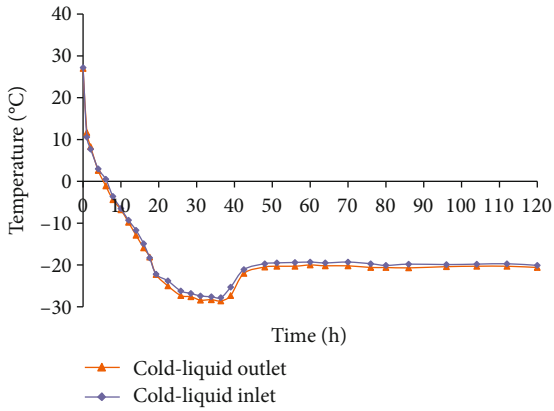

Figure 9: Variation law of cold source temperature.

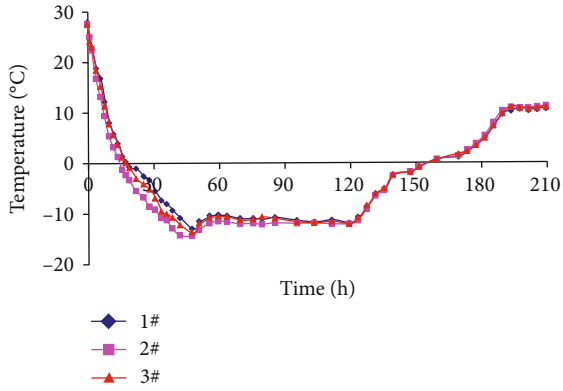

Figure 10: Temperature variation law of section I.

the whole freezing process is not more than 1°C, which ensures the smooth running of the test.

4.3.2. Temperature Variation Law of Section I. As shown in Figure 10, the three monitoring points ($1_{\#}$, $2_{\#}$, and $3_{\#}$) of temperature monitoring section I are affected by four tangential and axially adjacent frozen pipes, and the frozen model test of the inclined shaft lasts 210 h from the beginning to the end. During the whole freezing process, the temperature of each measuring point can be divided into four stages. The first is a rapid cooling stage. In this stage, the temperature cools from 27.4°C to 0°C at 1.37°C/h, and the lowest temperature is -15.6°C at 48 h. At this time, the temperature of each measuring point in section I is higher than -10°C, and the test is changed from the active freezing period to the maintenance freezing period. The second stage is a stationary stage. In this stage, due to the fact that the temperature of the cold source is stabilized, the temperature of each measuring point in section I is stabilized at 56 h after a small temperature rise, and now the freezing enters the maintenance period. The third stage is a rapid heating stage. The freezing was stopped at 120 h; then, the temperature of each measuring point in section I starts to rise rapidly and rises from -12.1°C to 0°C at 34 h at 0.38°C/h. At 194 h, the temperature of each measuring point in section I rises to the highest, and the highest temperature is 11.8°C. The fourth stage is a stable stage, in which

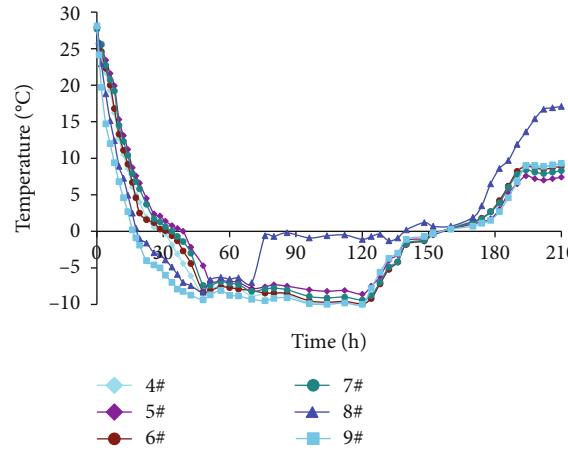

Figure 11: Temperature variation law of section II.

the temperature of each measuring point in section I is stable with an average temperature of 11.1°C.

4.3.3. Temperature Variation Law of Section II. Section II consists of 6 measuring points, namely, $4_{\#}$, $5_{\#}$, $6_{\#}$, $7_{\#}$, $8_{\#}$, and $9_{\#}$, which are used to monitor the temperature change of sand at the edge zone of the model test. The $4_{\#}$ and $6_{\#}$ measuring points to the shaft axis distance are equal, the $5_{\#}$ and $7_{\#}$ measuring points to the shaft axis position are equal, and the $8_{\#}$ and $9_{\#}$ measuring points are located at the ends of the shaft. The temperature of each measuring point varies with time, as shown in Figure 11. Figure 11 shows that the temperature of each measuring point in section II can be divided into four stages during the whole freezing process, namely, rapid cooling stage, stationary stage, rapid heating stage, and stable stage. The cooling speed of $4_{\#}$ and $6_{\#}$, $5_{\#}$ and $7_{\#}$, and $8_{\#}$ and $9_{\#}$ is the same, and the cooling speed is about 0.92°C/h, 0.82°C/h, and 1.57°C/h. The excavation at 76 h exposed the $8_{\#}$ measuring point which was exposed to air, and the temperature of the $8_{\#}$ measuring point was abrupt after 76 h.

4.3.4. Temperature Variation Law of Section III. Section III consists of four measuring points, namely, $10_{\#}$, $11_{\#}$, $12_{\#}$, and $13_{\#}$, which are used to monitor the temperature change of sand between two adjacent tangential frozen pipes. The temperature of each measuring point changes with time, as shown in Figure 12.

Figure 12 shows that the temperature variation of each measuring point in section III is basically the same as that of section I and section II during the whole freezing process, and both have a rapid cooling stage, stationary stage, rapid heating stage, and stable stage. The temperature variation of each measuring point in section III is basically the same, and the cooling rate is about 2.79°C/h. When the test changes from the active freezing period to the maintenance freezing period, the temperature of each measuring point in section III is smaller than that of other two sections, because the position of each measuring point in section III is closer to the freezing pipe, and the obtained cooling capacity is larger.

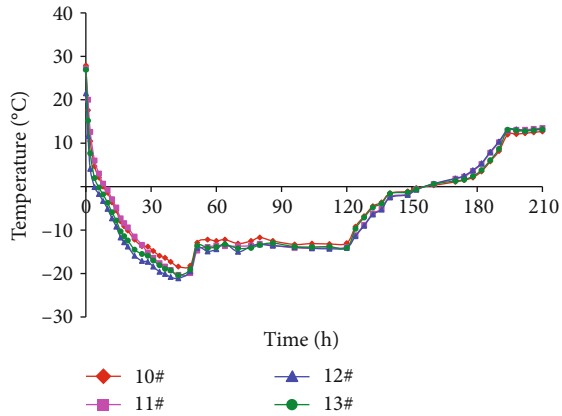

Figure 12: Temperature variation law of section III.

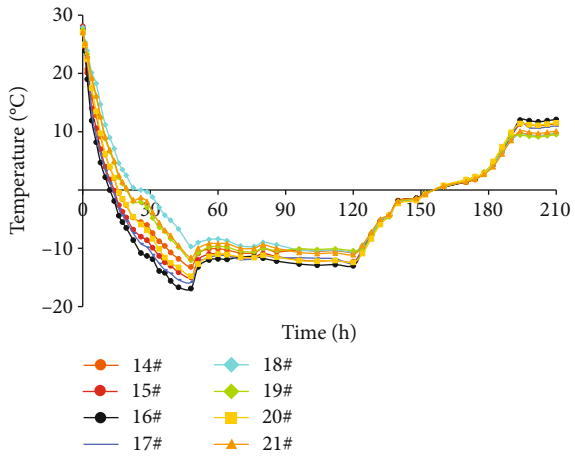

Figure 13: Temperature variation law of section IV.

4.3.5. Temperature Variation Law of Section IV. Section IV consists of 8 measuring points to monitor the temperature change of sand between two adjacent frozen pipes in the axial direction. The temperature of each measuring point changes with time, as shown in Figure 13. Figure 13 shows that the temperature variation of each measuring point in section IV is the same as that of section I, section II, and section III during the whole freezing process, and both have a rapid cooling stage, stationary stage, rapid heating stage, and stable stage. The temperature variation of each measuring point in section IV is the same, and the cooling rate is about 1.96°C/h.

In summary, the cooling rate of section III is fastest, and the second is section IV followed by section I. Section II is slowest, because the distance of section III to the cold source is smaller than that of section IV and the distance of section IV to the cold source is smaller than that of section I. Moreover, the distance of section I to the cold source is smaller than that of section II. The distance away from the cold source has a great influence on the cooling rate.

4.4. Frozen Wall Cooling Formula. The mechanical properties of the frozen wall change most during the active freezing period. The study on the temperature-time relationship of the frozen wall in the active freezing period can obtain the general cooling law of sand during the freezing process, which has a great significance to the prediction of frozen wall temperature. By fitting the relationship between the temperature and time of three typical sections in the positive freezing period, the formula for calculating the temperature-time of the frozen wall during the active freezing period can be obtained, which is shown in Figure 14.

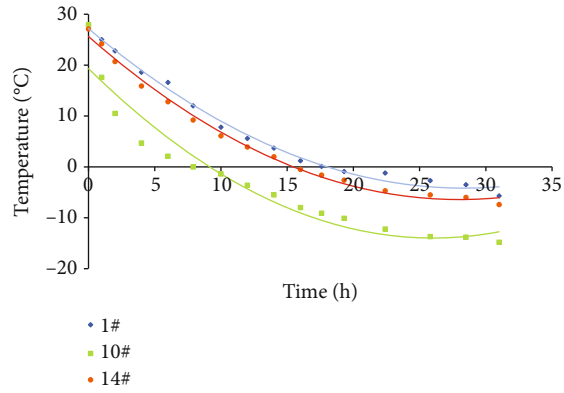

Figure 14: Temperature-time fitting curve of the frozen wall.

As shown in Figure 14, the freezing wall temperature and time are approximately quadratic parabolic and the fitting formula is as follows.

$$T = At^2 + Bt + C \tag{4}$$

In Formula (4), T is the freezing wall temperature (°C); t is the time (h); A, B, and C are parameters related to the distance between the measuring points and freezing pipe center.

The parameter values of A, B, and C are fitted from the relationship between the temperature data of temperature measurement points $1_{\#}$, $10_{\#}$, and $14_{\#}$ and the center of freezing pipes, as shown in Table 3.

After regression fitting the parameters A, B, and C, the relationship between parameters A, B, and C and center distance of the freezing pipe can be obtained:

$$\begin{aligned} A &= -2E^{-05}L^2 + 0.002L + 0.0113, \\ B &= 0.006L^2 - 0.0661L - 1.3291, \\ C &= 0.0074L^2 - 0.8143L + 32.887, \end{aligned} \tag{5}$$

The relationship between freezing wall temperature and time and the distance from the center of freezing pipes can be expressed as

$$\begin{aligned} T = {} & \left(-2E^{-05}L^2 + 0.002L + 0.0113\right)t^2 \\ & + \left(0.006L^2 - 0.0661L - 1.3291\right)t \\ & + 0.0074L^2 - 0.8143L + 32.887. \end{aligned} \tag{6}$$

In the formula, L is the distance between the measuring point and center of the freezing pipe (mm).

Table 3: Parameter values of A, B, and C.

Distance from the freezing pipe center (mm)	Measuring point	A	B	C	Correlation coefficient R^2
21	10#	0.0452	-2.4642	19.045	0.994
100	14#	0.0364	-2.1873	25.356	0.993
102.18	1#	0.0331	-2.0778	26.838	0.992

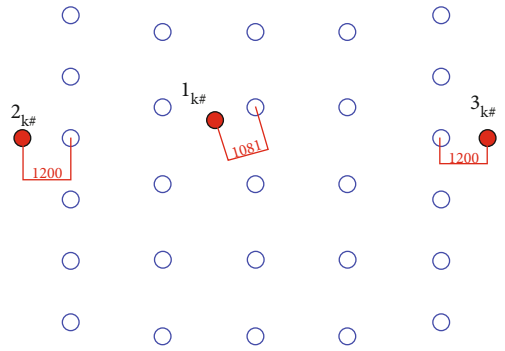

Figure 15: Layout of measuring points.

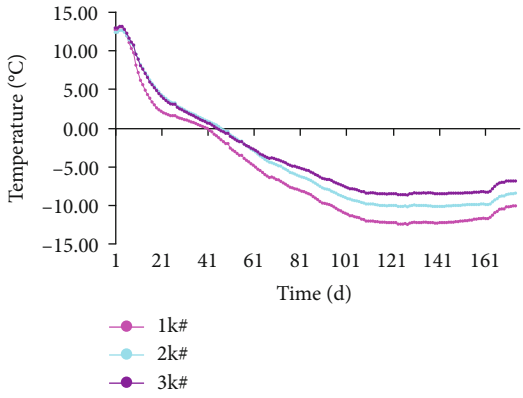

Figure 16: Measured temperature curve.

5. Field Measurement of Temperature Field Distribution of the Inclined Shaft Frozen Wall

The on-site temperature measurement points are arranged in the middle two rows and outside side rows of frozen pipes. There are three measuring points, which are shown in Figure 15. The $1_{k\#}$ measuring point is 1081 mm from the nearest frozen pipes, and the $2_{k\#}$ and $3_{k\#}$ measuring points are 1200 mm from the nearest frozen pipes.

The field temperature is shown in Figure 16. The cooling rate of sand is approximately linear with time during the active freezing period, and the temperature difference between three temperature measuring points is not large. The $1_{k\#}$ measuring point is closest to the frozen pipes, and its cooling rate is also fastest. The cooling rates of $2_{k\#}$ and $3_{k\#}$ measuring points are the same during the whole active freezing period. The cooling rates of $1_{k\#}$, $2_{k\#}$, and $3_{k\#}$ measuring points are 25.61 mm/d, 25.32 mm/d, and 25.35 mm/d, respectively, which indicates that the closer to the frozen pipe, the faster the cooling rate.

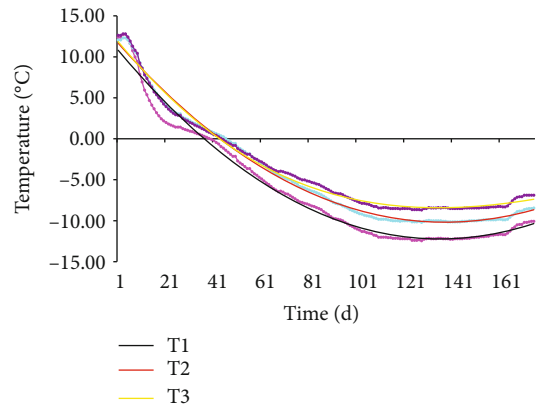

Figure 17: Comparison curve of calculated and measured temperature-time for the frozen wall.

To verify the cooling formula of the frozen wall, the calculated temperature by Formula (6) and field measured temperature of the frozen wall are drawn in the same figure (Figure 17). Figure 16 shows that the temperature calculated by Formula (6) fits well with the measured temperature of the frozen wall, indicating that Formula (6) can reflect the cooling law of the frozen wall during the active freezing period.

6. Conclusions

In this study, a three-dimensional physical simulation test system was developed to complete the test of temperature field distribution law of the artificially frozen inclined shaft. The experimental study on physical and mechanical properties of artificially frozen sand was completed; the results of this study can be summarized as follows:

With the cooling of frozen temperature (from 25°C to -20°C), the heat capacity of sand decreases first, increases second, then decreases, and finally tends to be stable. The thermal conductivity of sand gradually increases with the decrease in frozen temperature and finally becomes stable. The cohesion, internal friction angle, and uniaxial compressive strength of artificially frozen sand all increase. However, the amplitude of the increase will gradually decrease as the frozen temperature decreases, and the growth rate of uniaxial compressive strength is about 0.29~1.43 MPa/°C.

The variation of frozen wall temperature during the whole freezing process can be divided into four stages, and the closer to a frozen pipe, the faster the cooling rates. The cooling rate of section I is about 1.37°C/h, section II is about 0.92°C/h, section III is about 2.79°C/h, and section IV is about 1.96°C/h. The calculation formula of freezing wall temperature with time and distance from the center of freezing pipes of the inclined shaft is given.

The field measurement showed that the closer to the freezing pipe, the faster the cooling rates and the cooling rates of the $1_{k\#}$, $2_{k\#}$, and $3_{k\#}$ points were 25.61 mm/d, 25.32 mm/d, and 25.35 mm/d, respectively. The comparison of theoretical calculation results and field measurement results shows that the calculation formula of frozen wall temperature with time of the inclined shaft can reflect the general law of frozen wall temperature cooling.

The results of this study demonstrate that the self-made three-dimensional physical simulation test system in this paper is reliable, and the test method is feasible, which can reflect the general law of freezing inclined shaft cooling in a freezing inclined shaft.

Data Availability

All data generated or analyzed during this study are included within this article.

Conflicts of Interest

The authors declare that there is no conflict of interest regarding the publication of this paper.

Acknowledgments

This study is supported by the National Natural Science Foundation of China (No. 11872299), Natural Science Foundation of Shaanxi Province (No. 2019JQ-832), General Special Scientific Research Program of the Shaanxi Provincial Department of Education (No. 20JK0985), and Doctoral Research Start-Up Project of Yan'an University (No. YDBK2018-25).

References

[1] M. Qing-bin, H. Li-jun, S. Rong-jian et al., "Study and application of construction technology for inclined shafts penetrating drift sand strata in coal mine," *Chinese Journal of Geotechnical Engineering*, vol. 37, no. 5, pp. 900–910, 2015.

[2] G. Shao-hua, Y. Li, L. Zhen-Zhong, Q. Zhe, and N. Chuanxing, "Progress in research on reliability of inclined shaft frozen wall," *Coal Technology*, vol. 34, no. 10, pp. 49–51, 2015.

[3] J.-l. Fan, W. Yuan-chao, and W. Weiming, "Construction technology of freeze sinking method in inclined shaft soil layer," *Coal Science and Technology*, vol. 41, no. 9, pp. 143–150, 2013.

[4] C. Xiang-en and D. Chang-long, "Freezing construction technology of mine inclined shaft in mataihao mine," *Coal Science and Technology*, vol. 37, no. 11, pp. 21–23, 2009.

[5] Y. Zhang, J. Qiu, Y. Zhang, and Y. Wei, "The adoption of ELM to the prediction of soil liquefaction based on CPT," *Natural Hazards*, vol. 107, no. 1, pp. 539–549, 2021.

[6] Y. G. Zhang, J. Tang, R. P. Liao et al., "Application of an enhanced BP neural network model with water cycle algorithm on landslide prediction," *Stochastic Environmental Research and Risk Assessment*, vol. 35, pp. 1273–1291, 2020.

[7] Y. G. Zhang, J. Tang, Z. Y. He, J. Tan, and C. Li, "A novel displacement prediction method using gated recurrent unit model with time series analysis in the Erdaohe landslide," *Natural Hazards*, vol. 105, no. 1, pp. 783–813, 2020.

[8] Y. G. Zhang and L. Yang, "A novel dynamic predictive method of water inrush from coal floor based on gated recurrent unit model," *Natural Hazards*, vol. 105, no. 2, pp. 2027–2043, 2020.

[9] Y. G. Zhang, Z. Zhang, S. Xue, R. Wang, and M. Xiao, "Stability analysis of a typical landslide mass in the Three Gorges Reservoir under varying reservoir water levels," *Environmental Earth Sciences*, vol. 79, no. 1, 2020.

[10] Y. G. Zhang, S. Zhu, J. Tan, L. Li, and X. Yin, "The influence of water level fluctuation on the stability of landslide in the Three Gorges Reservoir," *Arabian Journal of Geosciences*, vol. 13, no. 17, p. 845, 2020.

[11] Y. G. Zhang, S. Zhu, W. Zhang, and H. Liu, "Analysis of deformation characteristics and stability mechanisms of typical landslide mass based on the field monitoring in the Three Gorges Reservoir, China," *Journal of Earth System Science*, vol. 128, no. 1, 2019.

[12] B. Gong, Y. J. Jiang, P. Yan, and S. Zhang, "Discrete element numerical simulation of mechanical properties of methane hydrate-bearing specimen considering deposit angles," *Journal of Natural Gas Science and Engineering*, vol. 76, p. 103182, 2020.

[13] B. Gong, Y. J. Jiang, and L. J. Chen, "Feasibility investigation of the mechanical behavior of methane hydrate-bearing specimens using the multiple failure method," *Journal of Natural Gas Science and Engineering*, vol. 69, p. 102915, 2019.

[14] C. Junjun, W. Wang, Z. Pengfei et al., "Analysis of artificial freezing temperature field for connected adit in water-rich sandy pebble stratum," *Railway Engineering*, vol. 59, no. 12, pp. 55–59, 2019.

[15] Y. Lin, Y. Zhaoming, and J. Zihua, "Artificial freezing tunnel model test and prediction of surrounding rock temperature field," *Sichuan Building Materials*, vol. 44, no. 8, pp. 66-67 +69, 2018.

[16] L. I. Yang, *Experimental Study on Thermal Conductivity of Artificial Frozen Clay and Develop Rules of Multi-Freezing-Tube Temperature Field*, AnHui University of Science and Technology, 2015.

[17] L. I. U. Bo, C. Yuchao, L. Dongyang, and S. Chang-jun, "Scale model tests and numerical analysis of artificial freezing at different temperatures in complicated strata," *Chinese Journal of Rock Mechanics and Engineering*, vol. 32, no. Z2, pp. 3328–3336, 2013.

[18] X. Hu and Z. Junjie, "Research on precision of Bakholdin model for temperature field of artificial ground freezing," *Chinese Journal of Underground Space and Engineering*, vol. 6, no. 1, pp. 96–101, 2010.

[19] L. Shuqing, "Numerical analysis of temperature field on artificial frozen wall," *Natural Science Journal of Harbin Normal University*, vol. 25, no. 3, pp. 43–45, 2009.

[20] H. Xiang-dong, H. Feng, and B. Nan, "Models of artificial frozen temperature field considering soil freezing point," *Journal of China University of Mining&Technology*, vol. 37, no. 4, pp. 550–555, 2008.

[21] W. Wenshun, W. J. Ping, J. Xuwen, W. Si-xian, and Y. Huiguang, "Experimental study of temperature field in course of artificial freezing," *Journal of China University of Mining&Technology*, vol. 33, no. 4, pp. 388–391+405, 2004.

[22] Z. Yan and Y. Songshui, "Using finite element method to analyze the formation and temperature distribution of the freezing-wall in the artificial freezing method," *Journal of Engineering Thermophysics*, vol. 2, pp. 175–181, 1984.

[23] W. Fan and P. Yang, "Ground temperature characteristics during artificial freezing around a subway cross passage," *Transportation Geotechnics*, vol. 20, p. 100250, 2019.

[24] Y.-j. Shen, Y.-z. Wang, X.-d. Zhao, G.-s. Yang, H.-l. Jia, and T.-l. Rong, "The influence of temperature and moisture content on sandstone thermal conductivity from a case using the artificial ground freezing (AGF) method," *Cold Regions Science and Technology*, vol. 155, pp. 149–160, 2018.

[25] G. Russo, A. Corbo, F. Cavuoto, and S. Autuori, "Artificial ground freezing to excavate a tunnel in sandy soil. Measurements and back analysis," *Research*, vol. 50, pp. 226–238, 2015.

[26] F. T. Yue, S. G. Lv, R. J. Shi, and Z. Yong, "Numerical analysis and spot-survey study of horizontal artificial ground freezing in tunnel connecting passage construction," *Applied Mechanics and Materials*, vol. 3843, 2015.

[27] M. Vitel, A. Rouabhi, M. Tijani, and F. Guérin, "Modeling heat transfer between a freeze pipe and the surrounding ground during artificial ground freezing activities," *Computers and Geotechnics*, vol. 63, pp. 99–111, 2015.

[28] Y. S. Kim, J.-M. Kang, J. Lee, S.-S. Hong, and K.-J. Kim, "Finite element modeling and analysis for artificial ground freezing in egress shafts," *KSCE Journal of Civil Engineering*, vol. 16, no. 6, pp. 925–932, 2012.

[29] Z.-q. Ji, X.-y. Xu, and Y. Lin-lin, "Study on the influence of artificial frozen soil layer to the temperature field and displacement field of the frozen wall," State Key Laboratory of Frozen Soil Engineering, 2006.

[30] R. Lackner, A. Amon, and H. Lagger, "Artificial ground freezing of fully saturated soil: thermal problem," *Journal of Engineering Mechanics*, vol. 131, no. 2, pp. 211–220, 2005.

[31] W. Yan-sen, H. Jia-hui, Y. Wei-hao, R. Yan-long, and S. Lei, "Temperature measurement of outer shaft wall during freezing sinking in deep alluvium," *Journal of China University of Mining & Technology*, vol. 35, no. 4, pp. 468–472, 2006.

[32] H. O. U. Yun-bing, J. Jin-fend, Z. Yi-Xin, and W. Heng, "Simulation study on freezing temperature field with multi row freezing tubes in construction of large cross section mine inclined shaft," *Coal Engineering*, vol. 12, pp. 77–80, 2012.

[33] W. Yong and Y. Wei-hao, "Study on mechanical law of freezing inclined shaft lining in topsoil during frozen wall thawing," *Coal Science and Technology*, vol. 44, no. 5, pp. 133–139, 2016.

[34] B. Liu, L. I. Yan, D. Hua-dong, and Y. Wei-dong, "Study on temperature field distribution law of freezing wall for inclined shaft," *Coal Science and Technology*, vol. 40, no. 12, pp. 4–7, 2012.

[35] Y. Zhao-ming, L. Zheng-fei, and C. Jun-hao, "Study on support vector machine method prediction of artificial ground freezing temperature field," *Coal Engineering*, vol. 9, pp. 87–89, 2012.

[36] Z. Wei, S. Bin, S. Wen-bin, C. Yi, and B. Wang, "Monitoring and application of distributed optical fiber sensors in transient temperature field of frozen soil," *Chinese Journal of Geotechnical Engineering*, vol. 5, pp. 723–728, 2007.

[37] L. Fang-zheng and X. Ming-ping, "Study on analytical solution of temperature field of artificial frozen soil by exponent-integral function," *Journal of Southeast University (Natural Science Edition)*, vol. 4, pp. 469–473, 2004.

[38] R. Jian-xi, S. Jie-long, Z. Kun, J. Wang, and D. Wang, "Study of mechanical properties and temperature field of inclined frozen wall in water-rich sand stratum," *Rock and Soil Mechanics*, vol. 38, no. 5, pp. 1405–1412, 2017.

[39] X. He, D. De-bing, Z. Xiaomin, and T. Wang, "Numerical analysis and field monitoring on the frozen temperature field of vertical hole in the inclined shaft," *Mining Research and Development*, vol. 37, no. 11, pp. 94–98, 2017.

[40] S. Tian-bao and W. Shi-yi, "Measurement and engineering application of temperature field multiple-ring hole frozen wall in extra-thick clay strata," *Chinese Journal of Geotechnical Engineering*, vol. 34, no. 8, pp. 1516–1521, 2012.

[41] R.-h. Wang and W. Wang, "Analysis for features of the freezing temperature field under deflective pipes," *Chinese Journal of Geotechnical Engineering*, vol. 25, no. 6, pp. 658–661, 2003.